Inorganic Chemistry
Article

Inorg. Chem. **2010**, *49*, 805–814 **805**
DOI: 10.1021/ic900203x

Luminescent Mononuclear Ag(I)−Bis(diphosphine) Complexes: Correlation between the Photophysics and the Structures of Mononuclear Ag(I)−Bis(diphosphine) Complexes

Kenji Matsumoto,[‡] Takao Shindo,[†] Naoki Mukasa,[†] Toshiaki Tsukuda,[†] and Taro Tsubomura*[,†]

[†]*Department of Materials and Life Science, Seikei University, 3-3-1 Kichijoji-kitamachi, Musashino, Tokyo, 180-8633, Japan and* [‡]*Department of Chemistry, Faculty of Science, Graduate School, Kyushu University, Hakozaki, Higashi-ku, Fukuoka 812-8581, Japan*

Received February 2, 2009

Correlation between the photophysics and the structures of three Ag(I)−bis(diphosphine) complexes ($[Ag(dppbz)_2]NO_3$ (**1**·**NO$_3$**), $[Ag(dppe)_2]NO_3$ (**2**·**NO$_3$**), and $[Ag(dppp)_2]NO_3$ (**3**·**NO$_3$**) (dppbz = 1,2-bis(diphenylphosphino)benzene, dppe = 1,2-bis(diphenylphosphino)ethane, dppp = 1,3-bis(diphenylphosphino)propane) has been investigated using temperature-dependent emission measurements and electrochemical and theoretical methods. All three Ag(I)−bis(diphosphine) complexes have relatively low oxidation potential, which allows metal-to-ligand charge transfer (MLCT) contribution in the lowest excited state of the tetrahedral geometry, which is difficult in other Ag(I) complexes. Both **1**·**NO$_3$** and **2**·**NO$_3$** show orange phosphorescence with moderate quantum yield in air-free methanol at room temperature, while **3**·**NO$_3$** is less emissive in solution at room temperature. In all three complexes the temperature-dependent luminescence measurements in EtOH/MeOH 4:1 (v/v) solution indicate the blue-shift of the emission maximum and the increase of the emission intensity on lowering the temperature. In particular, the sequential emission spectral change with decreasing temperature is observed in **1**·**NO$_3$** and **2**·**NO$_3$**. In the glass state at 90 K, all three complexes show intense blue phosphorescence. The theoretical calculation using density functional theory (DFT) suggests that the orange and blue emissions mainly originate from the ^{3}MC excited state based on a square-planar geometry and the ^{3}IL+^{3}MLCT excited state based on a tetrahedral geometry, respectively.

Introduction

A large number of the luminescent metal complexes have been studied for the past decades.[1,2] Among them in recent years, d^{10}-metal complexes are anticipated as emissive materials,[3] imaging probes,[4] and photocatalysts[5] because of their superior photophysical properties.[6] In particular, multinuclear d^{10}-metal complexes show interesting photoluminescence properties such as luminescence thermochromism, which are achieved by the control of metal−metal bonding interaction.[7] Although there are many reports on luminescent d^{10}-metal complexes, emissive mononuclear Ag(I) complexes have not been studied well because of their potential photosensitivity and limited luminescent property.[6,8]

Most recently, it has been reported that the Ag(I) complex with 1,2-bis(diphenylphosphino)benzene (dppbz), **1**·**PF$_6$**, shows

*To whom correspondence should be addressed. E-mail: tsubomura@st.seikei.ac.jp. Phone: +81-422-37-3752. Fax: +81-422-37-3871.

(1) *Photochemistry and Photophysics of Coordination Compounds I and II*; Balzani, V., Campagna, S. Eds.; Springer-Verlag: Heidelberg, 2007.
(2) Evans, R. C.; Douglas, P.; Winscom, C. J. *Coord. Chem. Rev.* **2006**, *250*, 2093–2126.
(3) (a) Tsubomura, T.; Ito, Y.; Inoue, S.; Tanaka, Y.; Matsumoto, K.; Tsukuda, T. *Inorg. Chem.* **2008**, *47*, 481–486. (b) Yam, V. W.-W.; Cheng, E. C.-C. *Top. Curr. Chem.* **2007**, *281*, 269. (c) Miller, A. J. M.; Dempsey, J. L.; Peters, J. C. *Inorg. Chem.* **2007**, *46*, 7244–7246. (d) Tsuboyama, A.; Kuge, K.; Furugori, M.; Okada, S.; Hoshino, M.; Ueno, K. *Inorg. Chem.* **2007**, *46*, 1992–2001. (e) Armaroli, N.; Accorsi, G.; Holler, M.; Moudam, O.; Nierengarten, J.-F.; Zhou, Z.; Wegh, R. T.; Welter, R. *Adv. Mater.* **2006**, *18*, 1313–1316.
(4) Barnard, P. J.; Wedlock, L. E.; Baker, M. V.; Berners-Price, S. J.; Joyce, D. A.; Skelton, B. W.; Steer, J. H. *Angew. Chem., Int. Ed.* **2006**, *45*, 5966–5970.
(5) (a) Tsubomura, T.; Sakai, K. *Coord. Chem. Rev.* **1998**, *171*, 107–113. (b) Horvárth, O. *Coor. Chem. Rev.* **1994**, *135*/*136*, 303–324. (c) Li, D.; Che, C.-M.; Kwong, H.-L.; Yam, V. W.-W. *J. Chem. Soc., Dalton Trans.* **1992**, 3325–3329.
(6) Barbieri, A.; Accorsi, G.; Armaroli, N. *Chem. Commun.* **2008**, 2185–2193.
(7) (a) Omary, M. A.; Colis, J. C. F.; Larochelle, C. L.; Patterson, H. H. *Inorg. Chem.* **2007**, *46*, 3798–3800. (b) Mohamed, A. A.; Burini, A.; Fackler, J. P. *J. Am. Chem. Soc.* **2005**, *127*, 5012–5013. (c) Catalano, V. J.; Moore, A. L. *Inorg. Chem.* **2005**, *44*, 6558–6566. (d) Rasika Dias, H. V.; Diyabalanage, H. V. K.; Rawashdeh-Omary, M. A.; Franzman, M. A.; Omary, M. A. *J. Am. Chem. Soc.* **2003**, *125*, 12072–12073.
(8) (a) Teets, T. S.; Partyka, D. V.; Esswein, A. J.; Updegraff, J. B., III.; Zeller, M.; Hunter, A. D.; Gray, T. G. *Inorg. Chem.* **2007**, *46*, 6218–6220. (b) Xie, L. X.; Wei, M. L.; Duan, C. Y.; Sun, Q. Z.; Meng, Q. J. *Inorg. Chim. Acta* **2007**, *360*, 2541. (c) Kunkely, H.; Vogler, A. *Inorg. Chim. Acta* **2006**, *359*, 388–390. (d) Lin, Y.-Y.; Lai, S.-W.; Che, C.-M.; Fu, W.-F.; Zhou, Z.-Y.; Zhu, N. *Inorg. Chem.* **2005**, *44*, 1511–1524.

Published on Web 01/07/2010

an interesting luminescence property.[9] The complex luminesces orange phosphorescence at room temperature, and when the temperature decreases until the media is frozen, the emission changes to intense blue. This phenomenon is known as luminescence thermochromism and occurs when the geometries differ at high and low temperatures.[10] In general, it is established that some d^{10}-metal complexes with tetrahedral geometry, such as Cu(I)-bis(diimine) complexes, show flattening distortion in their triplet metal-to-ligand charge transfer (^{3}MLCT) excited state because the d^9 configuration, which is caused by the charge transfer, prefers a square-planar geometry.[11] Therefore it has been deduced that the orange and blue emissions observed at room temperature and low temperature originate from square-planar and tetrahedral structures, respectively.

Most of the luminescent Ag(I) complexes, however, show emission due to cluster-centered or ligand-centered excited states.[6] Since an Ag(I) ion is inert to oxidation, the low-energy MLCT state hardly occurs.[8c] In fact, the absorption spectrum of $\mathbf{1 \cdot PF_6}$ is similar to that of the free ligand, dppbz, and the accurate assignment of the absorption is difficult. This is in contrast with luminescent Cu(I) complexes whose emission states are frequently assigned to MLCT. In addition, although in tetrahedral Cu(I) complexes the flattening distortion in the excited state leads to marked reduction of the luminescence intensity, $\mathbf{1 \cdot PF_6}$ shows a lower-energy and longer-life emission in solution (λ^{em}_{max} = 670 nm and τ = 11 μs in air-free 2-MeTHF)[9] with relatively strong intensity than that of the Cu(I) analogue, $[Cu(dppbz)_2]BF_4$ (λ^{em}_{max} = 556 nm and τ = 244 ns in air-free CH_2Cl_2).[12] This result shows that $\mathbf{1 \cdot PF_6}$ in the excited state has an extraordinarily slow deactivation rate.

We have been interested in the luminescent mononuclear d^{10} metal complexes and reported the photophysical properties of Pd(0),[3a] Pt(0),[3a,13] Cu(I),[14] and Au(I).[15] In recent years, we have also been studying the luminescence properties of mononuclear Ag(I) complexes. Interestingly, although it has been reported that the Ag(I) complex with dppe that is a dppbz analogue, $\mathbf{2 \cdot PF_6}$, is non-emissive in solution,[16] we discovered that the complex in degassed solution showed orange phosphorescence similar to $\mathbf{1 \cdot PF_6}$. The luminescent properties of three Ag(I)-bis(diphosphine) complexes (diphosphine = dppbz, dppe, dppp, Chart 1) which have different electronic and structural properties were investigated using electrochemical and temperature-dependent emission measurements and computational method. As a result, we found that these Ag(I) complexes have interesting emission properties which are different from Cu(I) complexes. In this report, luminescence details of the mononuclear Ag(I) complexes are discussed.

Chart 1

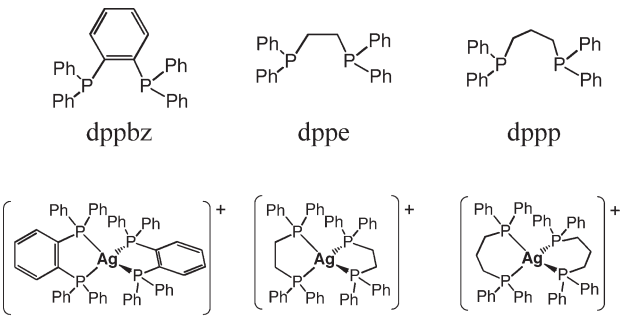

Experimental Section

General Procedures. Reagents and solvents were purchased from commercial suppliers and used without further purification unless otherwise noted. Elemental analyses were performed for C, H, and N elements on a Perkin-Elmer model 2400. $^{31}P\{^1H\}$ and ^1H NMR spectra were taken by a JEOL Lambda 400 Fourier transform spectrometer with Air-VT thermocontroller. The references of $^{31}P\{^1H\}$ and ^1H NMR spectra are external 85% H_3PO_4 and internal tetramethylsilane, respectively.

Synthesis of Complexes. To a methanol solution (50 mL) containing 1 mmol of a diphosphine ligand (dppbz, dppe, or dppp) was added a small amount of aqueous solution of silver(I) nitrate ($AgNO_3$; 0.5 mmol), and the mixture was stirred for 2 h under dark. After stirring, most of the solvent in the reaction solution was evaporated and then was cooled. The white powder of $[Ag(diphosphine)_2]NO_3$ was precipitated after cooling for several hours. The precipitate was filtered off and washed with diethyl ether. The complex obtained was recrystallized by slow diffusion of ether into the ethanol solution of a complex. The $^{31}P\{^1H\}$ and ^1H NMR spectra of $\mathbf{1 \cdot NO_3}$, $\mathbf{2 \cdot NO_3}$ and $\mathbf{3 \cdot NO_3}$ are depicted in the Supporting Information, Figures S1−S6.

$[Ag(dppbz)_2]NO_3$ ($\mathbf{1 \cdot NO_3}$). Anal. Calcd. for $C_{60}H_{48}Ag_1P_4N_1O_3$: C, 67.81; H, 4.55; N, 1.32. Found: C, 67.76; H, 4.45; N, 1.17. $^{31}P\{^1H\}$ NMR (160 MHz, CD_3OD): δ = 1.94 ($^1J_{AgP}$ = 230, 267 Hz). ^1H NMR (400 MHz, CD_3OD): δ = 7.61−7.55 (m, 8H, Ph), δ = 7.38−7.34 (m, 8H, Ph), δ = 7.18−7.13 (m, 32H, Ph).

$[Ag(dppe)_2]NO_3$ ($\mathbf{2 \cdot NO_3}$). Anal. Calcd. for $C_{52}H_{48}Ag_1P_4N_1O_3$: C, 64.61; H, 5.00; N, 1.45. Found: C, 64.51; H, 4.83; N, 1.58. $^{31}P\{^1H\}$ NMR (160 MHz, CD_3OD): δ = 4.31 ($^1J_{AgP}$ = 232, 267 Hz). ^1H NMR (400 MHz, CD_3OD): δ = 7.43−7.24 (m, 40H, Ph), δ = 2.55−2.52 (m, 8H, CH_2).

$[Ag(dppp)_2]NO_3$ ($\mathbf{3 \cdot NO_3}$). Anal. Calcd. for $C_{54}H_{52}Ag_1P_4N_1O_3$: C, 65.20; H, 5.27; N, 1.41. Found: C, 64.87; H, 5.31; N, 1.59. $^{31}P\{^1H\}$ NMR (160 MHz, CD_3OD): δ = −4.88 ($^1J_{AgP}$ = 217, 253 Hz). ^1H NMR (400 MHz, CD_3OD): δ = 7.40−7.21 (m, 40H, Ph), δ = 2.53 (br, 8H, P−CH_2), δ = 1.68 (br, 4H, −CH_2−).

Photophysics. Absorption and emission spectral measurements were carried out using degassed solutions by repeated freeze−pump−thaw procedures (at least five times). Absorption and emission spectra were measured with a Shimadzu UV-3100PC

(9) Osawa, M.; Hoshino, M. *Chem. Commun.* **2008**, 6384–6386.
(10) (a) Rubén, J.; Díez, A.; Fernández, J.; Forniés, J.; García, A.; Gil, B.; Lalinde, E.; Moreno, M. T. *Inorg. Chem.* **2008**, *47*, 7703–7716. (b) Felder, D.; Nierengarten, J.-F.; Barigelletti, F.; Ventura, B.; Armaroli, N. *J. Am. Chem. Soc.* **2001**, *123*, 6291–6299. (c) Ford, P. C.; Cariati, E.; Bourassa, J. *Chem. Rev.* **1999**, *99*, 3625–3647. (d) Wrighton, M.; Morse, D. L. *J. Am. Chem. Soc.* **1974**, *96*, 998–1003.
(11) (a) Armaroli, N. *Chem. Soc. Rev.* **2001**, *30*, 113–124. (b) Iwamura, M.; Takeuchi, S.; Tahara, T. *J. Am. Chem. Soc.* **2007**, *129*, 5248–5256.
(12) Moudam, O; Kaeser, A.; Delavaux-Nicot, B.; Duhayon, C.; Holler, M.; Accorsi, G.; Armaroli, N.; Séguy, I.; Navarro, J.; Destruel, P.; Nierengarten, J.-F. *Chem. Commun.* **2007**, 3077–3079.
(13) Abedin-Siddique, Z.; Ohno, T.; Nozaki, K.; Tsubomura, T. *Inorg. Chem.* **2004**, *43*, 663–673.
(14) (a) Tsukuda, T.; Nishigata, C.; Arai, K.; Tsubomura, T. *Polyhedron* **2009**, *28*, 7–12. (b) Saito, K.; Arai, T.; Takahashi, N.; Tsukuda, T.; Tsubomura, T. *Dalton Trans.* **2006**, 4444–4448. (c) Saito, K.; Tsukuda, T.; Tsubomura, T. *Bull. Chem. Soc. Jpn.* **2006**, *79*, 437–441. (d) Tsukuda, T.; Nakamura, A.; Arai, T.; Tsubomura, T. *Bull. Chem. Soc. Jpn.* **2006**, *79*, 288–290.
(15) Saito, K.; Tsukuda, T.; Matsumoto, K.; Tsubomura, T. *Bull. Chem. Soc. Jpn.* **2007**, *80*, 533–535.
(16) Delfs, C. D.; Kitto, H. J.; Stranger, R.; Swiegers, G. F.; Wild, S. B.; Willis, A. C.; Wilson, G. J. *Inorg. Chem.* **2003**, *42*, 4469–4478.

spectrophotometer and an Ocean Optics QE-65000 scientific-grade CCD spectrometer, respectively. A grating-monochromated Xe lamp source (lamp: AMKO, Lamphousing A 1000 series; monochromator: Jovin-Ybon, HR 320) was used for the excitation of the samples. Excitation and solid-state emission spectra were recorded by a Shimadzu RF-5000 fluorometer. The low-temperature solid-state emission spectral measurement was carried out using a SUPRASIL quartz tube and a quartz Dewar flask. The temperature-dependent emission spectral measurement in an air-free EtOH/MeOH 4:1 (v/v) solution was performed using a custom-made LN_2 cryostat (Jecc-Torisha) with a thermocontroller (Scientific Instruments, Model 9700). Unless otherwise noted, the temperature-dependent emission spectra and lifetimes were measured after over 40 min when a temperature has been set. All emission spectra were corrected using the LS-1-CAL calibration light source (Ocean Optics). The quantum yields (Φ) of $\mathbf{1\cdot NO_3}$, $\mathbf{2\cdot NO_3}$, and $\mathbf{3\cdot NO_3}$ were calculated by the following equation:[17]

$$\Phi = \Phi^*\left(\frac{n}{n^*}\right)^2\left(\frac{S}{S^*}\right)\left(\frac{I^*}{I}\right)\left(\frac{A^*}{A}\right)$$

where n is the refractive index of the solvent, S is the area of the corrected emission spectra, I is the intensity of light at the excitation wavelength, and A is the absorbance at the excitation wavelength. The asterisk refers to the standard sample. The excitation wavelengths for $\mathbf{1\cdot NO_3}$, $\mathbf{2\cdot NO_3}$, and $\mathbf{3\cdot NO_3}$ are 330, 312, 300 nm, respectively. Quinine bisulfate in 1 N H_2SO_4 was used for the standard of the quantum yield ($\Phi^* = 0.546$)[18] and was excited at the same wavelength for each complex (i.e., $I^*/I = 1$). At the excitation wavelength, the absorbance of all samples except for $\mathbf{3\cdot NO_3}$ is less than 0.1. Since the emission intensity of $\mathbf{3\cdot NO_3}$ is very weak, the value of a slightly larger absorbance (0.16) was used. Luminescence decay curves were measured on a laboratory-made apparatus; the sample was excited with a Nd:YAG laser (266 nm; Continuum, Minilite), and the emission light was focused into a Jovin-Ybon H-20 monochromator equipped with a photomultiplier (Hamamatsu, R-955). The output of the photomultiplier was acquired by a Tektronix TDS 5034 Digital Phosphor Oscilloscope.

Electrochemistry. The cyclic voltammetry of $\mathbf{1\cdot NO_3}$, $\mathbf{2\cdot NO_3}$, and $\mathbf{3\cdot NO_3}$ was carried out under the following conditions: [Ag(I) complex] = 1 mM, 100 mM tetra-*n*-butylammonium hexafluorophosphate (^{n}Bu$_4$NPF$_6$) as supporting electrolyte, a glassy carbon working electrode, an Ag/Ag^+ reference electrode, a Pt wire counter electrode, scan rate 100 mV/s. ^{n}Bu$_4$NPF$_6$ was recrystallized from hot acetonitrile before use. Before the measurement, deaeration of the solution was carried out using Ar bubbling during at least 15 min. The voltammogram was taken by a potentiostat (Huso Electrochemical System, HECS 311B 15−01) with a potential sweep unit (Huso Electrochemical System, HECS 321B) and was recorded using a *X*-*Y* recorder (Riken Denshi, Model F-35CA). The chart was digitalized by a graph reading software. The potential value obtained for the Ag/Ag^+ reference electrode scale was converted to the Fc/Fc^+ scale using the redox potential of Fc/Fc^+ obtained in the same condition as the external reference.

X-ray Crystallographic Analysis. A single crystal was mounted in a loop with liquid paraffin. An X-ray diffraction measurement was made on a Rigaku Saturn CCD area detector with graphite monochromated Mo-$K\alpha$ radiation, operating at 50 kV and 40 mA at −150 °C. Data were collected and processed on a PC using CrystalClear software (Rigaku) and was corrected for Lorentz and polarization effects. All calculations were performed using the CrystalStructure[19] (Ver. 3.8) crystallographic software package. The structure was solved using SIR92[20] and refined with program SHELXL-97.[21] The non-hydrogen atoms were refined anisotropically. The hydrogen atoms were refined isotropically. Molecular plot was obtained with the program ORTEP-3.[22] The crystallographic data are given in Supporting Information, Table S1.

Computational Details. All theoretical calculations were performed using Gaussian 03[23] for Windows (Ver. 6.1, Revision E-.01) on the Intel Core2 Quad Q6600 2.4 GHz computer with 2 GB memories. Both geometry optimization by density functional theory (DFT) and time-dependent DFT (TD-DFT)[24,25] calculations applied Becke's 3-parameter hybrid function[26] combined with the Lee−Yang−Parr correlation function[27] (B3LYP), and the basis set as follows: silver, CEP-121G; phosphorus, 6-31+G*; carbon, 6-31G*; hydrogen, 6-31G. No symmetry was used. In the calculation of the triplet state, unrestricted B3LYP (UB3LYP) was used. In the calculation of the singlet state, the "UltraFine" option was specified for the "Int" keyword. In the geometry optimization of all complexes, the atomic coordinates based on the crystal structure were used as the initial geometry. The modified GDIIS algorithm[28] was used as the optimization method. No solvent effect was included for the geometry optimization. In both geometry optimizations of the singlet and triplet states all four items (Maximum Force, rms Force, Maximum Displacement and rms Displacement) were converged or a maximum force became negligible small. The lowest 20 (for $Ag(dppe)_2$ and $Ag(dppp)_2$) or 30 (for $Ag(dppbz)_2$) singlet excited states were calculated for the optimized geometry in the singlet state using TD-DFT. The lowest 10 triplet excited states were computed for each optimized geometry in the triplet (for $Ag(dppbz)_2$) and singlet states (for all complexes). The SCF keyword options were specified as follows: "Tight, VShift = 500, Maxcycle = 256". The solvent effect using polarizable continuum model[29] (PCM) was included in the singlet excited energy calculation, and the chosen solvent was methanol. The input and output files for all calculations are described in the Supporting Information. The abbreviations in the figures and tables are as follows: ES, excited state; *f*,

(17) Demas, J. N.; Crosby, G. A. *J. Phys. Chem.* **1971**, *75*, 991.
(18) Parker, C. A.; Rees, W. T. *Analyst* **1960**, *85*, 581.
(19) *CrystalStructure Analysis Package*; Rigaku and Rigaku/MSC: 9009 New Trails Dr., The Woodlands, TX 77381, 2000−2006.
(20) Altomare, A.; Cascarano, G.; Giacovazzo, C.; Guagliardi, A.; Burla, M.; Polidori, G.; Camalli, M. *J. Appl. Crystallogr.* **1994**, *27*, 435.
(21) Sheldrick, G. M. *SHELXL-97*; University of Göttingen: Göttingen, Germany, 1997.
(22) Farrugia, L. J. *J. Appl. Crystallogr.* **1997**, *30*, 565.
(23) Frisch, M. J.; Trucks, G. W.; Schlegel, H. B.; Scuseria, G. E.; Robb, M. A.; Cheeseman, J. R.; Montgomery, Jr., J. A.; Vreven, T.; Kudin, K. N.; Burant, J. C.; Millam, J. M.; Iyengar, S. S.; Tomasi, J.; Barone, V.; Mennucci, B.; Cossi, M.; Scalmani, G.; Rega, N.; Petersson, G. A.; Nakatsuji, H.; Hada, M.; Ehara, M.; Toyota, K.; Fukuda, R.; Hasegawa, J.; Ishida, M.; Nakajima, T.; Honda, Y.; Kitao, O.; Nakai, H.; Klene, M.; Li, X.; Knox, J. E.; Hratchian, H. P.; Cross, J. B.; Bakken, V.; Adamo, C.; Jaramillo, J.; Gomperts, R.; Stratmann, R. E.; Yazyev, O.; Austin, A. J.; Cammi, R.; Pomelli, C.; Ochterski, J. W.; Ayala, P. Y.; Morokuma, K.; Voth, G. A.; Salvador, P.; Dannenberg, J. J.; Zakrzewski, V. G.; Dapprich, S.; Daniels, A. D.; Strain, M. C.; Farkas, O.; Malick, D. K.; Rabuck, A. D.; Raghavachari, K.; Foresman, J. B.; Ortiz, J. V.; Cui, Q.; Baboul, A. G.; Clifford, S.; Cioslowski, J.; Stefanov, B. B.; Liu, G.; Liashenko, A.; Piskorz, P.; Komaromi, I.; Martin, R. L.; Fox, D. J.; Keith, T.; Al-Laham, M. A.; Peng, C. Y.; Nanayakkara, A.; Challacombe, M.; Gill, P. M. W.; Johnson, B.; Chen, W.; Wong, M. W.; Gonzalez, C.; and Pople, J. A. *Gaussian 03*, Revision E.01; Gaussian, Inc.: Wallingford, CT, 2004.
(24) Bauernschmitt, R.; Ahlrichs, R. *Chem. Phys. Lett.* **1996**, *256*, 454.
(25) Hirata, S.; Head-Gordon, M. *Chem. Phys. Lett.* **1999**, *302*, 375.
(26) Beck, A. D.J. *Chem. Phys.* **1992**, *96*, 2155–2160. (b) Becke, A. D.J. *Chem. Phys.* **1993**, *98*, 5648–5652.
(27) Lee, C.; Yang, W.; Parr, R. G. *Phys. Rev.* **1988**, *B37*, 785.
(28) (a) Csaszar, P.; Pulay, P. *J. Mol. Struct.* (*Theochem*) **1984**, *114*, 31. (b) Farkas, Ö.; Schlegel, H. B. *J. Chem. Phys.* **1999**, *111*, 10806.
(29) (a) Miertus, S.; Scrocco, S.; Tomashi, J. *Chem. Phys.* **1981**, *55*, 117. (b) Cossi, M.; Barone, V.; Cammi, R.; Tomasi, J. *Chem. Phys. Lett.* **1996**, *255*, 327. (c) Cossi, M.; Rega, N.; Scalmani, G.; Barone, V. *J. Comput. Chem.* **2003**, *24*, 669.

Table 1. Photophysical and Electrochemical Properties of $\mathbf{1}\cdot\mathbf{NO_3}$, $\mathbf{2}\cdot\mathbf{NO_3}$, and $\mathbf{3}\cdot\mathbf{NO_3}$

complex	λ^{abs}_{max}/nm[a] (ε/M^{-1} cm^{-1})	λ^{em}_{max} at 295 K/nm[a] (τ/μs)	λ^{em}_{max} at 90 K/nm[b] (τ/μs)	Φ/%[a]	E_{ox}/V[c] (vs Fc/Fc$^+$)	E_{red}/V[c] (vs Fc/Fc$^+$)
$\mathbf{1}\cdot\mathbf{NO_3}$	273 (3.6×10^4)	680 (28), 445[d]	445 (2.4×10^3)	8.3	+0.48 (+0.36)[f]	+0.42
$\mathbf{2}\cdot\mathbf{NO_3}$	263 (3.7×10^4)	693 (12)	403 (1.1×10^4)	4.2	+0.64 (+0.44)[f]	+0.45
$\mathbf{3}\cdot\mathbf{NO_3}$	268 (3.2×10^4)	ca.430 (n. d.)[e]	410 (9.9×10^3)	<0.05	+0.86 (+0.39)[f]	

[a] In air-free methanol. [b] In air-free EtOH/MeOH 4:1 (v/v). [c] In Ar-saturated acetonitrile. [d] In solid. [e] Not determined. [f] Oxidation potential of the corresponding free ligand.

Table 2. Calculated Singlet Excited States and Their Transition Energies Related to the Absorption Spectra of $\mathbf{1}^+$, $\mathbf{2}^+$, and $\mathbf{3}^+$[a]

complex	no. of excited state	calculated transition/nm	oscillator strength	main transition (maximum CI coefficient)	assign
$\mathbf{1}^+$	ES 7	295.24	0.1011	242 HOMO−1 → 244 LUMO (0.66346)	^{1}IL + ^{1}MLCT
	ES 18	270.57	0.1605	243 HOMO → 255 LUMO+11 (0.51487)	^{1}IL + ^{1}MLCT
$\mathbf{2}^+$	ES 1	292.50	0.1769	219 HOMO → 220 LUMO (0.53506)	^{1}IL + ^{1}MLCT
	ES 10	271.69	0.2052	219 HOMO → 224 LUMO+4 (0.58034)	^{1}IL + ^{1}MLCT
$\mathbf{3}^+$	ES 1	288.80	0.1280	227 HOMO → 228 LUMO (0.55992)	^{1}IL + ^{1}MLCT
	ES 12	262.36	0.1518	227 HOMO → 234 LUMO+6 (0.58691)	^{1}IL + ^{1}MLCT

[a] All calculation results are deposited in the Supporting Information

oscillator strength; CI coeff., configuration interaction coefficient.

Results and Discussion

$\mathbf{1}\cdot\mathbf{NO_3}$, $\mathbf{2}\cdot\mathbf{NO_3}$, and $\mathbf{3}\cdot\mathbf{NO_3}$ were prepared by the reaction of a methanol solution of each corresponding diphosphine with an aqueous solution of $AgNO_3$ and obtained them in good yield (ca. 80%). The $^{31}P\{^1H\}$ NMR spectra of $\mathbf{1}\cdot\mathbf{NO_3}$, $\mathbf{2}\cdot\mathbf{NO_3}$, and $\mathbf{3}\cdot\mathbf{NO_3}$ in $CDCl_3$ show two doublets centered at δ 1.12 ($^1J_{AgP}$ = 230 and 265 Hz), 3.90 ($^1J_{AgP}$ = 232 and 263 Hz), and −5.39 ($^1J_{AgP}$ = 226 and 257 Hz), respectively, in which the splitting is attributed to the two isotopes of silver, ^{107}Ag and ^{109}Ag, having each 1/2 of nuclear spin. Their signals in the complexes show downfield shifts compared with those of free diphosphines (dppbz: δ −13.4, dppe: δ −12.0, dppp: δ −17.0). The measurement in a coordinating solvent, methanol-d_4, also gave similar results (see also the Experimental Section). These results indicate that the four phosphorus atoms in those complexes are magnetically equivalent and Ag−P bonds are not fluxional in solution on the NMR time-scale.

The single crystal of $\mathbf{1}\cdot\mathbf{NO_3}$ was obtained by diffusing ether into its chloroform solution. The cation in the complex of $\mathbf{1}\cdot\mathbf{NO_3}$ has a C_2-symmetry and adopts a distorted tetrahedral geometry (Supporting Information, Figure S7). The crystallographic data are shown in Supporting Information, Table S1. The Ag−P lengths and P−Ag−P angle are 2.4560(4) and 2.5103(4) Å and 80.055(13)°, respectively. These values are almost identical to those of the corresponding PF_6 salt, $\mathbf{1}\cdot\mathbf{PF_6}$.[9] The dihedral angle between the two P−Ag−P planes is 85°, indicating that the two chelate planes are almost orthogonal to each other. These values are within the range of typical Ag(I)−phosphine complexes.[9,30]

The absorption spectra of $\mathbf{1}\cdot\mathbf{NO_3}$, $\mathbf{2}\cdot\mathbf{NO_3}$, and $\mathbf{3}\cdot\mathbf{NO_3}$ in methanol at room temperature are shown in Supporting Information, Figure S8. The photophysical and electrochemical properties of these Ag(I)-bis(diphosphine) complexes are summarized in Table 1. All complexes have an intense absorption band (ε = ca. 35,000 M^{-1} cm^{-1}) around 270 nm, which is similar to those of each ligand (dppbz: 277 nm (ε = 2.0×10^4 M^{-1} cm^{-1}) in EtOH/MeOH (4:1 v/v)[31a] and about 280 nm (ε = ca. 1.8×10^4 M^{-1} cm^{-1}) in 2-MeTHF,[9] dppe: 251 nm (ε = 1.83×10^4 M^{-1} cm^{-1}) in cyclohexane,[31b] dppp: 252 nm (ε = 1.76×10^4 M^{-1} cm^{-1}) in cyclohexane[31b]). This suggests that these bands involve an intraligand (IL) character. In addition, the shoulder bands are observed around 300 nm for all complexes. Since the lower-energy shoulder band is not observed in the absorption spectra of ligands, this may be attributed to an IL charge transfer perturbed from a metal center. Although many luminescent mononuclear Ag(I) complexes exclusively show IL excited states, these absorption bands are assigned as ^{1}IL transitions involving significant contribution of ^{1}MLCT. This is supported by TD-DFT calculations for the three Ag(I)-bis(diphosphine) complexes discussed later. The results of the calculations suggest that there are some bands derived from mixed ^{1}IL and ^{1}MLCT from 260 to 300 nm (Supporting Information, Figure S9 and Table 2).

The cyclic voltammogram (CV) of three Ag(I)-bis(diphosphine) complexes in acetonitrile is depicted in Figure 1. The CV of $\mathbf{1}\cdot\mathbf{NO_3}$ shows a reversible redox wave with $E_{1/2}$ = +0.45 V versus Fc$^+$/Fc and ΔE = 0.06 V at room temperature. In $\mathbf{2}\cdot\mathbf{NO_3}$ the voltammogram gives an irreversible redox pair. The anodic (E_{pa}) and cathodic (E_{pc}) peak potentials of $\mathbf{2}\cdot\mathbf{NO_3}$ are +0.64 and +0.45 V versus Fc$^+$/Fc, respectively. The voltammogram of $\mathbf{3}\cdot\mathbf{NO_3}$ gave only an anodic peak at +0.86 V versus Fc$^+$/Fc. The redox potentials of Ag(I)-bis(diphosphine) complexes are significantly smaller than that of [Ag([18]aneS$_4$O$_2$)]PF$_6$ (E_{pa} = +1.09 V and E_{pc} = +0.95 V versus Fc$^+$/Fc at 253 K) whose ligand is able to form a stable Ag(II) complex.[32] The low redox potential of Ag(I)-bis(diphosphine) complexes may be attributed to stabilization of the divalent complexes by phosphine ligands

(30) (a) Affandi, D.; Berners-Price, S. J.; Effendy; Harvey, P. J.; Healy, P. C.; Ruch, B. E.; White, A. H. *J. Chem. Soc., Dalton Trans.* **1997**, 1411–1420. (b) Gimeno, M. C.; Jones, P. G.; Laguna, A.; Sarroca, C. *J. Chem. Soc., Dalton Trans.* **1995**, 1473. (d) Harker, C. S.W.; Tiekink, E. R. T. *J. Coord. Chem.* **1990**, *21*, 287.

(31) (a) This work. (b) Liaw, B.; Orchard, W.; Kutal, C. *Inorg. Chem.* **1988**, *27*, 1311–1316.

(32) Huang, D.; Blake, A. J.; McInnes, E. J. L.; McMaster, J.; Davies, E. S.; Wilson, C.; Wolowska, J.; Schröder, M. *Chem. Commun.* **2008**, 1305–1307.

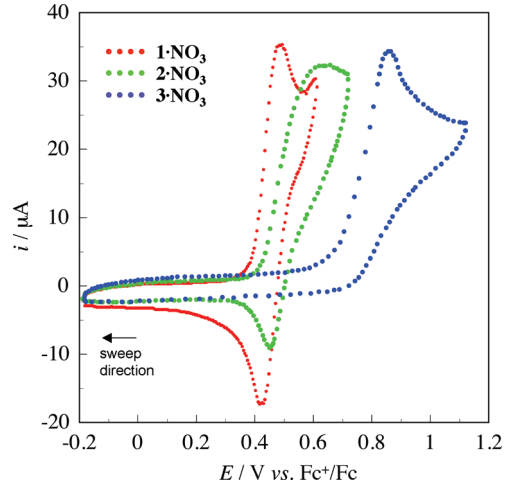

Figure 1. Cyclic voltammograms of Ag(I)-bis(diphosphine) complexes in acetonitrile at room temperature.

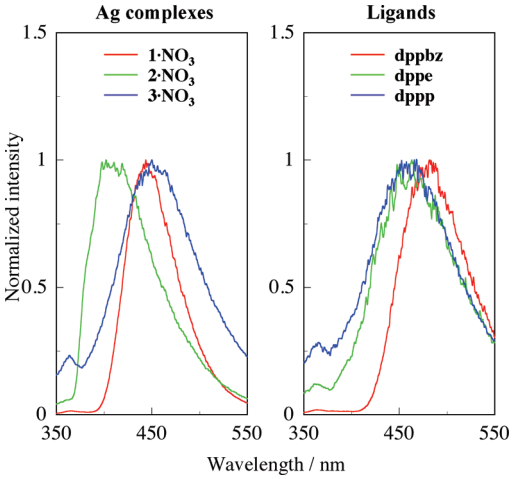

Figure 2. Emission spectra (uncorrected) of Ag(I)-bis(diphosphine) complexes (left) and corresponding ligands (right) in the solid state at 77 K.

having both σ-donor and π-acceptor characters.[32,33] Related ligands (dppbz, dppe, and dppp) show only an irreversible anodic peak around +0.4 V versus Fc^+/Fc (Table 1). The fact that a reversible redox pair is found in the CV of **1·NO$_3$** shows that the oxidation mechanism is different from that of the ligand oxidation. Such low oxidation potential and reversible redox process of the Ag(I) complex should be ascribed to significant contribution of metal orbitals to the highest occupied molecular orbital (HOMO), which is shown by the DFT results. This may explain why the Ag-phosphine complexes have the excited states with significant MLCT character, which is difficult in other Ag(I) complexes.

The room-temperature emission spectra of **1·NO$_3$**, **2·NO$_3$**, and **3·NO$_3$** are shown in Supporting Information, Figure S10. In the solid state **1·NO$_3$** indicates strong blue luminescence with peak maximum at 445 nm upon excitation at 300 nm, whereas **2·NO$_3$** and **3·NO$_3$** are almost non-

(33) (a) Shaw, J. L.; Wolowska, J.; Collison, D.; Howard, J. A. K.; McInnes, E. J. L.; McMaster, J.; Blake, A. J.; Wilson, C.; Schröder, M. *J. Am. Chem. Soc.* **2006**, *128*, 13827–13839. (b) Walker, N. R.; Wright, R. R.; Barran, P. E.; Murrell, J. N.; Stace, A. J. *J. Am. Chem. Soc.* **2001**, *123*, 4223–4227.

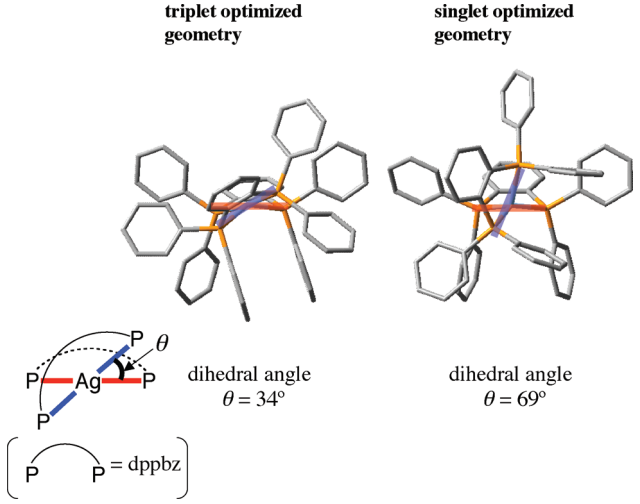

Figure 3. Comparison of the optimized geometries of **1**$^+$ in triplet and singlet states.

emissive. At 77 K all complexes are emissive in the solid state (Figure 2). In **1·NO$_3$** and **2·NO$_3$**, their emission maxima show slight blue-shifts in comparison with their free ligands. This result suggests that the IL excited state is perturbed by the metal. On the other hand, **3·NO$_3$** shows the same emission spectrum as the free ligand, indicating that the emission of **3·NO$_3$** in the solid state predominantly originates from the IL excited state.

Under oxygen-free condition, the methanol solutions of **1·NO$_3$** and **2·NO$_3$** show orange luminescence with peak maxima at 680 and 693 nm, respectively. The large Stokes shifts in solution suggest that the structures of these complexes in the excited state are considerably distorted from that in the ground state.

The luminescence quantum yields of **1·NO$_3$** and **2·NO$_3$** in methanol at room temperature are 8.3% and 4.2%, respectively. These values are significantly higher than other luminescent Ag(I) complexes,[2,6,8a] and the former is comparable to the value of **1·PF$_6$** in less coordinative solvent, 2-MeTHF.[9] The higher quantum yield of **1·NO$_3$** compared with **2·NO$_3$** may be attributed to the rigid structure with a phenylene group in the P−P chelate ring. Although it is well-known that the luminescence of many Cu(I) complexes involving Cu(I)-bis(diimine) complexes is quenched in the coordinating solvents such as nitriles and alcohols, this result indicates that these Ag(I)-bis(diphosphine) complexes in the excited state are not susceptible to the nucleophilic attack of the solvent molecules. The orange emissions of **1·NO$_3$** and **2·NO$_3$** in the solution state were completely quenched in the presence of oxygen. The emissions show the single exponential decay, and the emission lifetimes of **1·NO$_3$** and **2·NO$_3$** are 28 and 12 μs, respectively, indicating that these emissions have a phosphorescence nature. In the literature[16] it has been described that **2·PF$_6$** is non-emissive in solution. In the previous study the emission of the complex might be quenched by a trace amount of oxygen involved in the media. On the other hand, **3·NO$_3$** shows a very weak emission with a peak maximum around 430 nm, which significantly differs from the emission behaviors of **1·NO$_3$** and **2·NO$_3$**. Since the emission of **3·NO$_3$** in room-temperature solution resembles that of the ligand in the low-temperature solid, the emission band probably stems from an IL excited state.

Table 3. Observed and Calculated Triplet Transition Energies of $\mathbf{1}^+$, $\mathbf{2}^+$, and $\mathbf{3}^+$

	complex	solution at r. t.	glass at 90 K (solid at r. t.)
observed λ^{em}_{max}/nm	$Ag(dppbz)_2$	680	445 (445)
	$Ag(dppe)_2$	693	403
	$Ag(dppp)_2$	ca.430	410

		triplet-optimized geometry	singlet-optimized geometry (crystal structure)
calculated λ^{em}_{max}/nm	$Ag(dppbz)_2$	609.56	359.49 (356.15)
	$Ag(dppe)_2$	a	350.93
	$Ag(dppp)_2$	a	347.40

[a] Not calculated.

Calculation of the optimized geometry of $\mathbf{1}^+$ in the triplet state by the DFT method shows that it adopts a significantly flattened geometry (Figure 3). The dihedral angle between the two P−Ag−P planes of the triplet-optimized geometry of $\mathbf{1}^+$ is 34°, which is significantly smaller than the values for the singlet-optimized geometry (69°) and that found in the crystal (85°). The lowest triplet excitation energy for the triplet-optimized geometry using the TD-DFT method is consistent with the corresponding observed value (Table 3). The calculation also suggested that the emission band based on the flattening distorted geometry stems from the ^{3}MC excited state including MLCT such as a metal−phosphine $d\sigma^* \rightarrow p\pi$ transition (Figure 4, Table 4). The emission behavior of $\mathbf{2 \cdot NO_3}$ could be also explained in a similar way. Although, in general, for d^{10} metal ions the MC excited states lie at much higher energy, the square-planar geometry and the $p\pi-p\pi$ bonding interaction between Ag 5p and phosphine 3p orbitals in the lowest unoccupied molecular orbital (LUMO) may decrease the energy level of the MC excited states in $\mathbf{1 \cdot NO_3}$ and $\mathbf{2 \cdot NO_3}$ because the square-planar geometry significantly raises the energy level of the $d_{x^2-y^2}$ orbital of silver atom compared to the tetrahedral geometry and the $p\pi-p\pi$ bonding interaction decreases the energy level of the silver 5p orbital (Supporting Information, Figure S11). Therefore, such $p\pi-p\pi$ bonding interaction stabilizes a structure of the complex in the excited state, which leads to the high quantum yields of $\mathbf{1 \cdot NO_3}$ and $\mathbf{2 \cdot NO_3}$ compared with other luminescent Ag(I) complexes.

Interestingly, at 90 K, all three Ag(I) complexes in the glass state (EtOH/MeOH = 4:1) show intense blue and very long-lived luminescence (Supporting Information, Figure S12, Table 1). The emission spectra of all complexes are similar to those in the solid state at 77 K (Figure 2). This result suggests that the complexes excited at low temperature maintain the original (distorted tetrahedral) geometry. In fact, the lowest triplet excitation energies calculated by the TD-DFT method based on the singlet-optimized geometries and the crystal structure of $\mathbf{1}^+$ explain that the distorted tetrahedral complex exhibits blue-shifted phosphorescence compared to that of the flattened structure. (Table 3). Furthermore, it is suggested that the emission band based on the distorted tetrahedral geometry stems from admixture of ^{3}IL and ^{3}MLCT excited states (Supporting Information, Figure S13, Table 4). The calculation for the singlet-optimized geometries of $\mathbf{2}^+$ and $\mathbf{3}^+$ also gave similar results. However, in the case of $\mathbf{3}^+$, the pure ^{3}IL character largely contributes to the excited

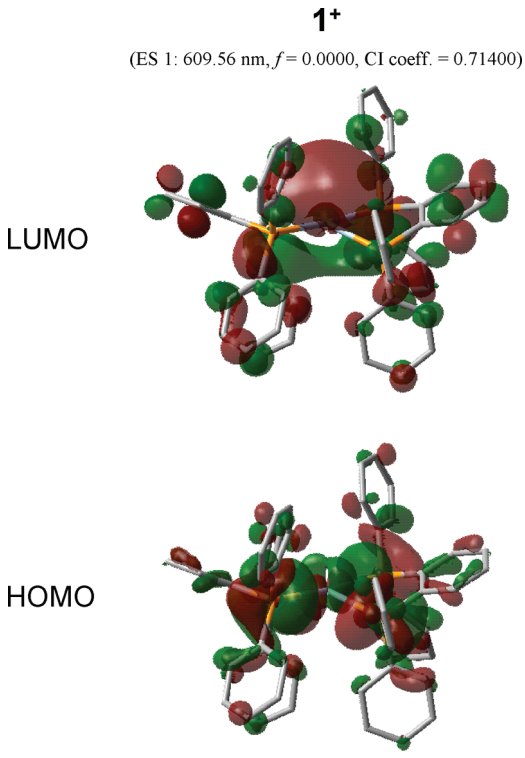

Figure 4. Molecular orbitals (isovalue = 0.02) related to the lowest triplet excitation based on the triplet-optimized geometry of $\mathbf{1}^+$. ES, excited state; *f*, oscillator strength; CI coeff., configuration interaction coefficient.

state in comparison with $\mathbf{1}^+$ and $\mathbf{2}^+$ (Table 4). In general, since the ^{3}IL excited state undergoes thermal deactivation at room temperature, $\mathbf{3 \cdot NO_3}$ may have poor luminescence. Since the structure of $\mathbf{3}^+$ is closer to an ideal tetrahedral geometry than that of $\mathbf{1}^+$ and $\mathbf{2}^+$, the relatively strong IL character in the excited state is probably attributed to the fact that the d-orbital splitting in $\mathbf{3}^+$ is smaller than that in $\mathbf{1}^+$ and $\mathbf{2}^+$.

Surprisingly, all excitation spectra at 90 K are consistent with those at room temperature (Figure 5), especially in $\mathbf{1 \cdot NO_3}$ and $\mathbf{2 \cdot NO_3}$, despite the large difference between the emission maxima at room temperature and 90 K. This result indicates that the absorption species corresponding to the emission bands at both room temperature and 90 K are the same. Thus, for $\mathbf{1 \cdot NO_3}$ and $\mathbf{2 \cdot NO_3}$, the results described here can be explained on the basis of flattening distortion which occurs in the excited state at room temperature, as expected from the theoretical calculation.

To investigate the temperature-dependence of media on the emission of mononuclear Ag(I)-bis(diphosphine) complexes, the temperature-dependent emission spectra of $\mathbf{1 \cdot NO_3}$, $\mathbf{2 \cdot NO_3}$, and $\mathbf{3 \cdot NO_3}$ were measured at various temperatures. As the temperature of the solution of $\mathbf{1 \cdot NO_3}$ decreases from 295 to 150 K, the intensity of emission increases, and the peak maximum shifts to longer wavelength up to 755 nm (Figure 6A). $\mathbf{2 \cdot NO_3}$ also shows a similar behavior (Figure 6C). Decrease of emission intensity has been often observed in some d^{10} complexes with a red-shift of emission maximum on lowering the temperature.[3a,d,10b] This observation is explained by the thermal equilibrium between singlet and triplet excited states.[10b,34] Since in $\mathbf{1 \cdot NO_3}$ and

(34) Siddique, Z. A.; Yamamoto, Y.; Ohno, T.; Nozaki, K. *Inorg. Chem.* **2003**, *42*, 6366–6378.

Table 4. Summary of the Calculated Lowest Triplet Transition for $\mathbf{1}^+$, $\mathbf{2}^+$, and $\mathbf{3}^{+a}$

complex	optimized geometry	transition energy / nm	top four transitions (contribution)	assign
$\mathbf{1}^+$	triplet	609.56	243 HOMO → 244 LUMO (100%)	^{3}MC
	singlet	359.49	243 HOMO → 246 LUMO+2 (34%) 243 HOMO → 244 LUMO (29%) 242 HOMO–1 → 247 LUMO+3 (11%) 241 HOMO–2 → 245 LUMO+1 (7%)	^{3}IL+^{3}MLCT
$\mathbf{2}^+$	singlet	350.93	219 HOMO → 220 LUMO (19%) 219 HOMO → 221 LUMO+1 (19%) 219 HOMO → 224 LUMO+4 (14%) 219 HOMO → 225 LUMO+5 (7%)	^{3}IL+^{3}MLCT
$\mathbf{3}^+$	singlet	347.40	227 HOMO → 234 LUMO+6 (21%) 227 HOMO → 236 LUMO+8 (15%) 227 HOMO → 230 LUMO+2 (9%) 221 HOMO–6 → 239 LUMO+11 (9%)	^{3}IL+^{3}MLCT ^{3}IL

[a] All calculation results are deposited in the Supporting Information.

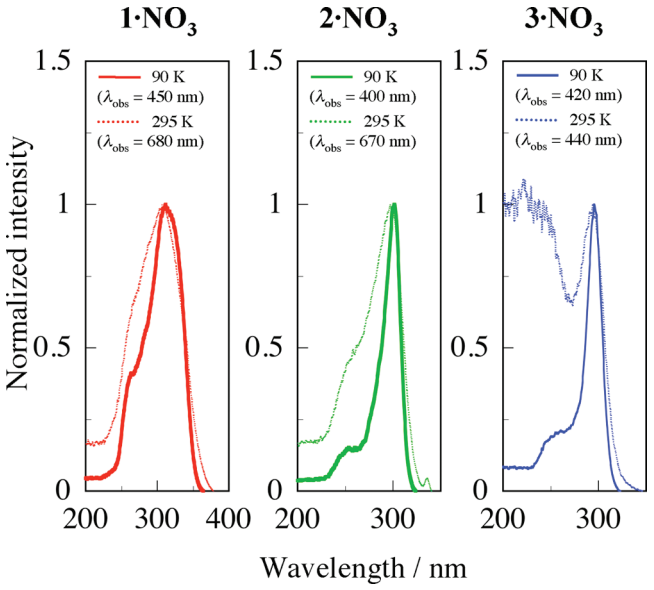

Figure 5. Excitation spectra (uncorrected) of Ag(I)-bis(diphosphine) complexes in an air-free EtOH/MeOH 4:1 (v/v) at room temperature (dotted line) and 90 K (solid line). [$\mathbf{1}\cdot\mathbf{NO_3}$] = 50 μM, [$\mathbf{2}\cdot\mathbf{NO_3}$] = 66 μM, and [$\mathbf{3}\cdot\mathbf{NO_3}$] = 59 μM.

$\mathbf{2}\cdot\mathbf{NO_3}$ both emission intensities increase on lowering the temperature, the observed red-shift is not attributed to such thermal equilibrium. On the other hand, it is well-known that the Cu(I)−bis(2,9-dimethyl-1,10-phenanthroline) complex shows large Stokes shift in a non-coordinative solvent at room temperature, and this is attributed to the structural change of the complex from tetrahedral to square-planar geometries in the excited state.[11b] Considering these findings, the red-shift found in $\mathbf{1}\cdot\mathbf{NO_3}$ and $\mathbf{2}\cdot\mathbf{NO_3}$ may be caused by the change in the average geometry of the complex with temperature in the excited state, that is, in a cooled solution adopts a more flattened geometry than that in a solution at room temperature. Under 150 K, as shown in Figure 6B, the emission shows sequential blue-shift with multicolor emission spectral change and becomes intense and long-lived as temperature decreases (Figure 7 and Supporting Information, Table S2). The phenomenon that the emission color sequentially changes from red to blue is unprecedented. Similar emission behavior is also found in $\mathbf{2}\cdot\mathbf{NO_3}$ although in a narrow temperature range from 100 to 90 K the sequential blue-shift occurs. (Figure 6D). Interestingly, in both cases a rise in the emission intensity after the excitation is observed in the same temperature range (Figure 8). The observed rise-times of $\mathbf{1}\cdot\mathbf{NO_3}$ at 110 K and $\mathbf{2}\cdot\mathbf{NO_3}$ at 100 K are 5 and 7 μs, respectively. In addition, the emission intensity after the rise decays single exponentially. In $\mathbf{2}\cdot\mathbf{NO_3}$, especially, the rise of the emission is found in the lower-energy emission band but not in the higher-energy one (Figure 8 (iv) inset). Since the absorption species corresponding to both lower- and higher-energy emission bands are the same (vide supra), these results indicate that the structure of a complex in the excited state slowly changes from a tetrahedral geometry showing a higher-energy emission band to a square-planar geometry showing a lower-energy emission band. The structural change in the excited state is generally much more rapid than the emission process.[11b] The observed risetimes are significantly long, which are comparable with the luminescence lifetimes. Similar behavior is found in tetranuclear copper(I) iodide clusters such as $[Cu_4I_4(4\text{-Phpy})_4]$ with different structures in different excited states (^{3}XLCT and ^{3}CC) which are poorly coupled.[35] In $\mathbf{1}\cdot\mathbf{NO_3}$ and $\mathbf{2}\cdot\mathbf{NO_3}$, hence, it is suggested that there are two different excited states (^{3}IL+^{3}MLCT and ^{3}MC) corresponding to two different structures (tetrahedral and square-planar geometries), and that the geometrical change occurs in a microsecond time scale at the specific temperature range (90−100 K). At the temperature range, the non-radiative deactivation of the excited state in the tetrahedral geometry and the change in the geometry into a more flattened one should occur with similar rates, and the radiative rate of the initially populated excited state should be far slower than the former two rates. With these conditions satisfied, the observed results, that is, the low-energy emission has a slow rise, may be reasonably explained. The blue-shift of the emission maximum in $\mathbf{1}\cdot\mathbf{NO_3}$ and $\mathbf{2}\cdot\mathbf{NO_3}$ on lowering the temperature may reflect the sequential suppression of the flattening distortion around the silver ion in the excited state.

(35) Kyle, K. R.; Ryu, C. K.; DiBenedetto, J. A.; Ford, P. C. *J. Am. Chem. Soc.* **1991**, *113*, 2954–2965.

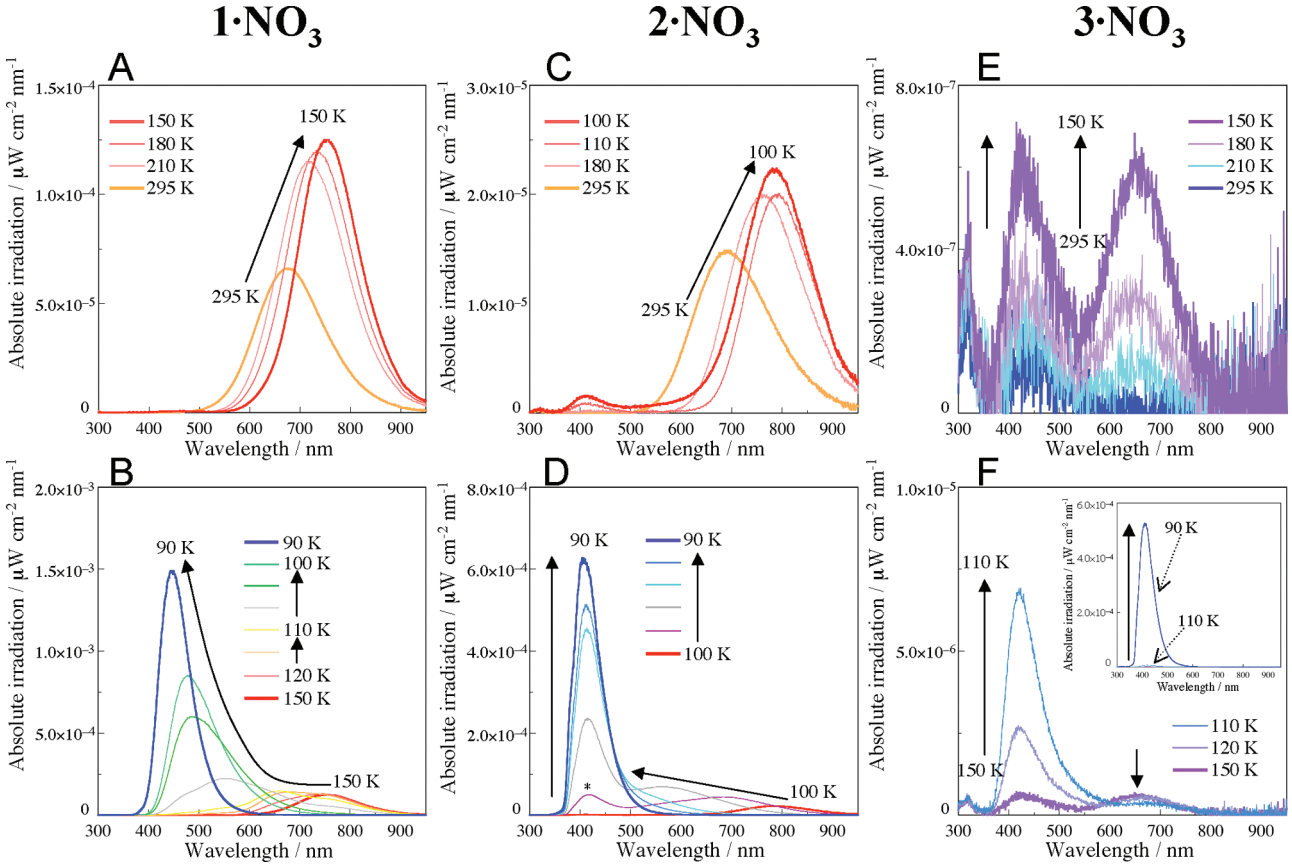

Figure 6. Temperature-dependent emission spectra of Ag(I)-bis(diphosphine) complexes in an air-free EtOH/MeOH 4:1 (v/v) solution. [**1**·NO_3] = 49 μM, [**2**·NO_3] = 50 μM, and [**3**·NO_3] = 55 μM.

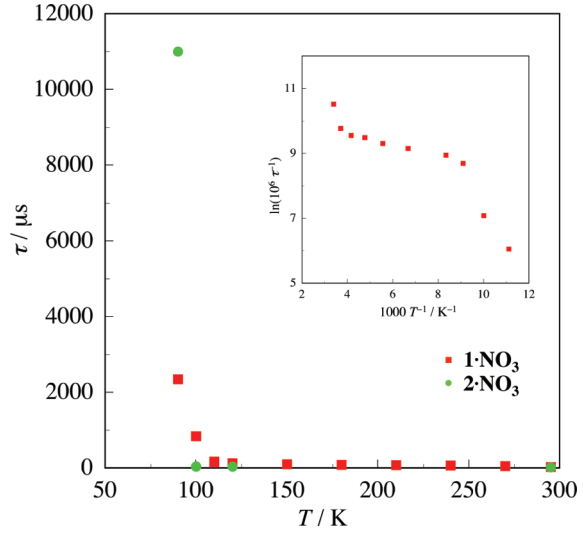

Figure 7. Temperature dependence of the emission lifetimes for **1**·NO_3 and **2**·NO_3 in the range from 295 to 90 K. Inset: Arrhenius plot of the emission lifetime for **1**·NO_3.

Such emission mechanism may lead to the complicated temperature dependence of the emission lifetime of **1**·NO_3 (Figure 7 inset).

In **3**·NO_3, in addition to a very weak emission band centered around 430 nm observed at room temperature, a new weak emission band with peak maximum around 680 nm similar to that for **1**·NO_3 and **2**·NO_3 appears on lowering the temperature. Since $\mathbf{3}^+$ adopts almost ideal tetrahedral geometry compared to $\mathbf{1}^+$ and $\mathbf{2}^+$ because of its large bite angle, in $\mathbf{3}^+$ the flattening distortion in the excited state may hardly occur by means of the large steric repulsion between the phenyl groups. The intensities of both emission bands slightly increase when the temperature decreases to 150 K (Figure 6E). The appearance of a lower-energy emission band in the range from 210 to 150 K may be attributed to the reduction of the non-radiative deactivation from the tetrahedral excited state with large ^{3}IL character and the stabilization of the flattening distorted state by decreasing temperature. Under 150 K, however, the intensity of only the higher-energy emission band remarkably increases, and the lower-energy emission band gently weakens (Figure 6F). This result also suggests that the flattening distortion of the complex in the excited state hardly occurs at low temperature.

From our findings, the mechanism of the emission for the three Ag(I)−bis(diphosphine) complexes, $\mathbf{1}^+$, $\mathbf{2}^+$, and $\mathbf{3}^+$, could be explained as shown in Chart 2. In $\mathbf{1}^+$ and $\mathbf{2}^+$ at room temperature, the complexes in the IL excited state with significant contribution of MLCT rapidly undergo the flattening distortion ($k_f \gg k_T$),[36] and then show the lower-energy emission originated from the ^{3}MC excited state based on square-planar geometry (in Chart 2, the route indicated by red arrows). At low temperature, since the flattening distortion does not essentially occur ($k_T \gg k_f$), the complexes emit the higher-energy luminescence stemming from the ^{3}IL+^{3}MLCT excited state based on the tetrahedral geometry (in Chart 2, the route indicated by blue arrows). In the intermediate state

(36) Hereat, an observed rate constant for the decay of the excited state indicates the sum of radiative and non-radiative rate constants.

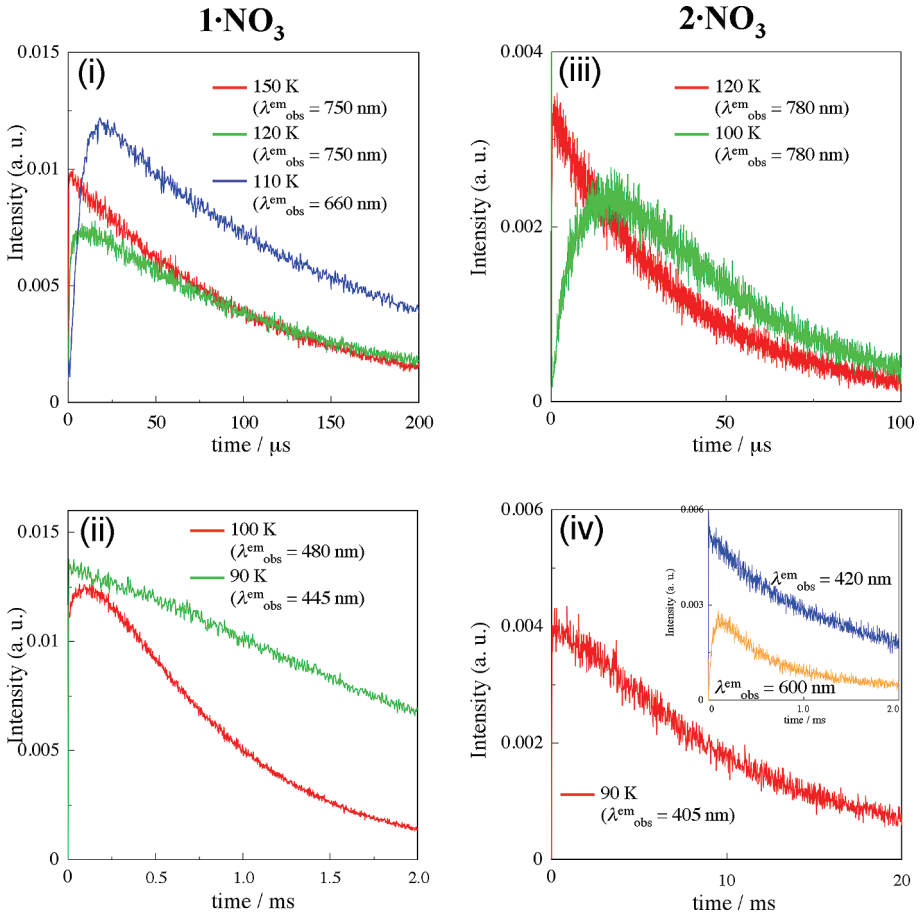

Figure 8. Emission decay of **1·NO3** and **2·NO3** in an air-free EtOH/MeOH 4:1 (v/v) solution at different temperatures. **1·NO3**: (i) 150, 120, and 110 K; (ii) 100 and 90 K. **2·NO3**: (iii) 120 and 100 K; (iv) 90 K. Inset: After 30 min when the temperature was set at 90 K (the spectrum with asterisk in Figure 6D).

Chart 2.[a]

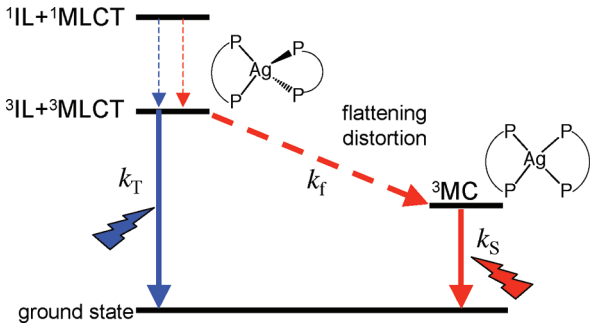

[a] k_T = Observed rate constant for the decay of the excited state from a tetrahedral geometry in rigid media. k_S = Observed rate constant for the decay of the excited state from a square−planar geometry in fluid media. k_f = Observed rate constant for the flattening distortion.

around the freezing point of media, the emission may occur from the species having the intermediate geometry depending on the temperature. On the other hand, in 3^+ at room temperature, since the pure ^{3}IL character largely contributes to the excited state in comparison with 1^+ and 2^+, non-radiative deactivation is predominant. At low temperature (but not below freezing point), since non-radiative deactivation is suppressed, in addition to the higher-energy emission, the lower-energy emission similar to that of 1^+ and 2^+ is observed (in Chart 2, the routes indicated by blue and red arrows). At sufficient low temperature, since non-radiative deactivation and flattening distortion are significantly suppressed ($k_T \gg k_f$), the higher-energy emission as well as 1^+ and 2^+ is found (in Chart 2, the route indicated by blue arrows).

Conclusion

We investigated the luminescence properties of three Ag(I)−bis(diphosphine) complexes, **1·NO3**, **2·NO3**, and **3·NO3**, using photophysical, electrochemical, and theoretical methods. These Ag(I) complexes have relatively low oxidation potential compared with other Ag(I) complexes. Not only **1·NO3** but also **2·NO3** operate as good orange triplet emitters in solution although 2^+ has been reported to be non-emissive in solution. On the other hand, **3·NO3** is less emissive in solution. In the EtOH/MeOH 4:1 (v/v) glass, all three complexes show intense blue phosphorescence. The theoretical calculation using DFT suggests that the orange and blue emissions mainly originate from the ^{3}MC excited state based on a square-planar geometry and the ^{3}IL+^{3}MLCT excited state based on a tetrahedral geometry, respectively. Furthermore, the temperature-dependent emission spectra of **1·NO3** and **2·NO3** indicate the sequential emission spectral change on lowering the temperature. A slow rise in the emission intensity after excitation is observed in the lower-energy emission. These results support the fact that there are two different excited states (^{3}IL+^{3}MLCT and ^{3}MC) corresponding to two different structures (tetrahedral and square-planar geometries), and slow flattening distortion

from the former to the latter structures occurs in a certain temperature range. These findings suggest that the mononuclear Ag(I)−bis(diphosphine) complexes flattened in the excited state is not susceptible to the nucleophilic attack of solvent molecules which frequently causes non-radiative deactivation in luminescent Cu(I) complexes. Therefore, Ag(I)−bis(diphosphine) complexes have a potential to show higher luminescence compared to Cu(I) complexes. In addition, as observed in **1·NO$_3$**, depending on temperature, the phenomenon in which a single complex shows luminescent color from red to blue is unprecedented. This interesting emission property may lead to the application to various luminescence sensors.

Acknowledgment. This work was financially supported by the Promotion and Mutual Aid Corporation for Private Schools of Japan through the Science Research Promotion Fund and through the High-tech Research Center Project.

Supporting Information Available: Additional figures, computational details, and crystallographic data for **1·NO$_3$** in CIF format. This material is available free of charge via the Internet at http://pubs.acs.org.